EPJ manuscript No.
(will be inserted by the editor)

The reflectivity of relativistic ultra-thin electron layers

Hui-Chun Wu and Jürgen Meyer-ter-Vehn

Max-Planck-Institut für Quantenoptik, D-85748 Garching, Germany

Received: date / Revised version:

Abstract. The coherent reflectivity of a dense, relativistic, ultra-thin electron layer is derived analytically for an obliquely incident probe beam. Results are obtained by two-fold Lorentz transformation. For the analytical treatment, a plane uniform electron layer is considered. All electrons move with uniform velocity under an angle to the normal direction of the plane; such electron motion corresponds to laser acceleration by direct action of the laser fields, as it is described in a companion paper (paper I). Electron density is chosen high enough to ensure that many electrons reside in a volume λ_R^3, where λ_R is the wavelength of the reflected light in the rest frame of the layer. Under these conditions, the probe light is back-scattered coherently and is directed close to the layer normal rather than the direction of electron velocity. An important consequence is that the Doppler shift is governed by $\gamma_x = (1-(V_x/c)^2)^{-1/2}$ derived from the electron velocity component V_x in normal direction rather than the full γ-factor of the layer electrons.

PACS. 52.38.Ph X-ray, γ-ray, and particle generation – 52.38.-f Intense particle beams and radiation source in physics of plasma – 52.59.Ye Plasma devices for generation of coherent radiation

1 Introduction

High intensity laser pulses have opened new possibilities to create dense electron sheets moving with velocity v_m close to velocity of light c implying a high relativistic factor $\gamma = (1-(v_m/c)^2)^{-1/2} \gg 1$. They can act as relativistic mirrors and Doppler-shift visible light to VUV- and X-ray frequencies by factors $4\gamma_m^2$ with high efficiency [1]. Also the pulse duration is reduced by the same amount, offering new options for atto-second physics.

Different methods exist to create relativistic mirrors. One way is to drive plasma waves in a gas jet laser plasma to the threshold of wave breaking. Non-linear plasma dynamics then form diverging density spikes moving with the group velocity of the driving laser pulse [2]. Light reflected from such wake fields has been detected recently, and $\gamma_x \approx 5$ could be inferred from the measured Doppler shift [3]. Another method is to reflect intense, linear-polarized laser pulses from solid surfaces. In this case, the light pressure drives electron oscillations at the critical surface of the over-dense laser plasma and forms an oscillating mirror [4]. It generates high harmonics spectra having universal properties which have been analyzed in [5,6]. The surface harmonics have been observed recently up to photon energies of 3.8 keV [7]. A third method is to irradiate ultra-thin foils [8,9] in a regime in which laser action separates all electrons from ions forming dense relativistic electron layers, as it has been described in a companion paper, referred to as paper I [10].

The present paper deals with the reflectivity of ultra-thin electron layers [11] and is closely related to paper I [10]. Originating from solid foils, the density of the electron layers is typically above the critical density. Nevertheless, they are transparent to optical light (and even more so to Doppler-shifted light in their rest frame), because the layer thickness is chosen smaller than the skin depth. The focus of this paper is on what fraction of probe laser energy is reflected and how does this reflectivity scale with layer density, thickness, and γ_m-factor.

Our particular interest is in coherent reflection. This takes place when a large number N of electrons resides in a volume λ_R^3, where λ_R is the wavelength in the rest frame of the layer. The scattered amplitudes then add coherently, and the reflected signal scales with N^2. This is what also happens in a partially reflecting, normal mirrors. It is in contrast to incoherent scattering, which scales $\propto N$ and produces much weaker reflection. Incoherent scattering from relativistic electrons was discussed in [12] and has been observed recently also from laser-driven relativistic electron bunches [13].

As another important difference, coherent emission is oriented along the normal direction of the relativistic electron layers and governed by the electron velocity component V_x, leading to Doppler shifts $\propto \gamma_x^2 = 1/(1-(V_x/c)^2)$. In contrast, incoherent emission is oriented along the momentum of individual scatterers with Doppler shift $\propto \gamma^2$. For layers driven directly by the laser field, electrons necessarily have large transverse momentum p_y, and $\gamma_x = \gamma/(1+(p_y/m_e c)^2)^{1/2}$ is typically much smaller than the full γ-factor. This leads to significantly reduced Doppler shifts.

In the following, we derive an analytic expression for coherent reflection of a probe pulse obliquely incident on a

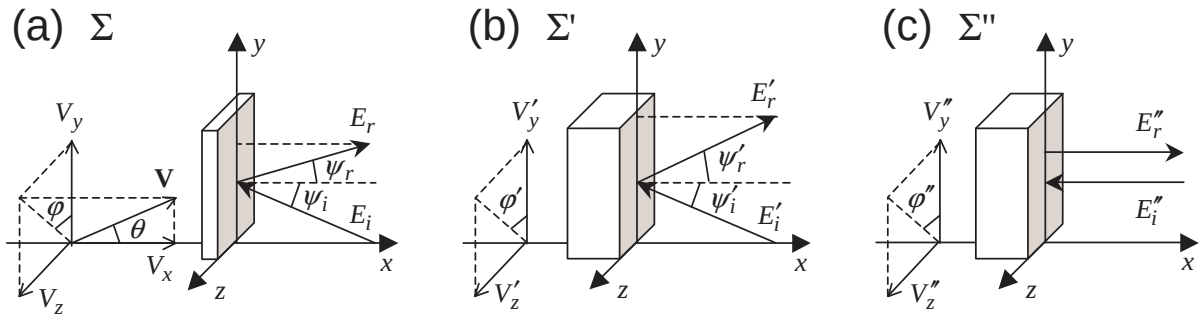

Fig. 1. Different frames and definition of symbols for probe light obliquely incident in (x, y) plane on a relativistic electron layer. The uniform layer consists of electrons, having velocity $\mathbf{V} = [V_x, V_y, V_z]$. (a) laboratory frame Σ, (b) intermediate frame Σ' boosted in x-direction such that $V'_x = 0$, (c) final fame Σ'', boosted in y-direction such that light is normally incident.

plane, uniform, relativistic electron layer driven by direct laser action. The linear reflectivity is considered, i.e. the probe pulse is chosen weak enough to neglect effects of the probe light on layer dynamics. Section 2 details two-fold Lorentz transformation into a frame in which the probe light is normally incident and $V_x = 0$. In this frame, linear coherent scattering is treated in one-dimensional geometry. The condition for coherent scattering is discussed. In Section 3, we compare the analytical results with one-dimension particle-in-cell (1D-PIC) simulations.

2 Lorentz transformation

We consider a plane dense electron layer moving at velocity V_x in normal x-direction with relativistic factor $\gamma_x = (1 - (V_x/c)^2)^{-1/2} > 1$. Fig. 1a illustrates the geometry in the laboratory frame Σ. The uniform layer consists of electrons, all having the same velocity

$$\mathbf{V} = [V_x, V_y, V_z] = V[\cos\theta, \sin\theta\cos\varphi, \sin\theta\sin\varphi]. \quad (1)$$

Probe light with amplitude E_i is incident from the right-hand side under an angle ψ_i relative to the normal. The x, y plane is chosen as plane of incidence; the incident light has wave vector $\mathbf{k}_i = k_i[-\cos\psi_i, \sin\psi_i, 0]$, and frequency $\omega_i = k_i c$.

The problem is to determine the amplitude E_r, the frequency ω_r, and the angle ψ_r of the reflected light. In order to solve the problem, we first perform a Lorentz transformation into frame Σ' (see Fig. 1b), moving into x-direction such that $V'_x = 0$. In a second transformation, we find frame Σ'' (see Fig. 1c) such that the probe light is incident normally. This second transformation was proposed by Bourdier [14] to treat oblique incidence in one-dimensional laser plasma configurations. We now give the transformation formulas explicitly, before treating the 1D reflection problem in Section 3.

2.1 $\Sigma \to \Sigma'$

Relative to the lab frame Σ, the intermediate frame Σ' moves with a longitudinal velocity $V_x\mathbf{e}_x$, where $\mathbf{e}_x$ is the unit vector in the x direction. In Σ', the mirror has only transverse velocity $\mathbf{V}' = \gamma_x[0, V_y, V_z]$, where $\gamma_x = (1 - \beta_x^2)^{-1/2}$ and $\beta_x = V_x/c$. Its relativistic factor becomes $\gamma' = \gamma/\gamma_x$. Thickness and density of the mirror are $d' = d\gamma_x$ and $n'_e = n_e/\gamma_x$, obtained from the transformation of the 4-vector $[n_e\mathbf{V}, n_e c]$.

In Σ', the field amplitude is $E'_i = E_i\gamma_x(1 + \beta_x\cos\psi_i)$, independent of the polarization direction. The incident light has frequency $\omega'_i = k'_i c = \omega_i\gamma_x(1 + \beta_x\cos\psi_i)$ and wave vector $\mathbf{k}'_i = k_i[-\gamma_x(\cos\psi_i + \beta_x), \sin\psi_i, 0]$. ¿From this one obtains the angle of incidence

$$\tan\psi'_i = \frac{\sin\psi_i}{\gamma_x(\cos\psi_i + \beta_x)}. \quad (2)$$

2.2 $\Sigma' \to \Sigma''$

Relative to Σ', the frame Σ'' moves with a transverse velocity $c\sin\psi'_i\mathbf{e}_y$. This special transformation is widely used to implement oblique incidence in 1D PIC codes [14]. It transforms obliquely incident into normally incident light. In the frame Σ'', the electron velocity is

$$\mathbf{V}'' = [0, V'_y - c\sin\psi'_i, V'_z\cos\psi'_i]/(1 - \beta'_y\sin\psi'_i), \quad (3)$$

and one has $\gamma'' = \gamma'(1 - \beta'_y\sin\psi'_i)/\cos\psi'_i$. The electron density becomes $n''_e = n'_e(1 - \beta'_y\sin\psi'_i)/\cos\psi'_i$. The layer thickness is $d'' = d'$.

For the incident light, we have $E''_i = E'_i\cos\psi'_i$, $\omega''_i = \omega'_i\cos\psi'_i$, and $\mathbf{k}''_i = [-k'_i\cos\psi'_i, 0, 0]$. So the angle of incidence is $\psi''_i = 0$. It is noted that there are two Lorentz invariants $E''_i/\omega''_i = E'_i/\omega'_i = E_i/\omega_i$ and $n''_e/\gamma'' = n'_e/\gamma' = n_e/\gamma$, which is the electron density in the rest frame of the mirror.

As we shall derive below, the reflected signal has $\mathbf{k}''_r = [k'_i\cos\psi'_i, 0, 0]$, $\omega''_r = \omega''_i$, and $\psi''_r = 0$. Its amplitude E''_r will be calculated in Sec. 3. The polarizations of E''_r and E''_i are the same.

2.3 $E''_r \to E'_r$

In frame Σ', we have $\omega'_r = \omega'_i$, $\mathbf{k}'_r = k'_i[\cos\psi'_i, \sin\psi'_i, 0]$, and $\psi'_r = \psi'_i$. This means the reflected wave has the same

frequency as the incident light and the reflection angle is equal to the angle of incidence. The field amplitude is $E'_r = E''_r/\cos\psi'_i$.

2.4 $E'_r \to E_r$

In the lab frame, the reflected signal has frequency $\omega_r = \omega'_i\gamma_x(1+\beta_x\cos\psi'_i)$ and wave vector $\mathbf{k}_r = k'_i[\gamma_x(\cos\psi'_i + \beta_x), \sin\psi'_i, 0]$. Using ω'_i obtained in Sec. 2.1, one gets the Doppler shift

$$\omega_r = \omega_i\gamma_x^2(1+\beta_x\cos\psi_i)(1+\beta_x\cos\psi'_i). \quad (4)$$

¿From the wave vector $\mathbf{k}_r$ one finds the reflection angle ψ_r in the form

$$\tan\psi_r = \frac{\sin\psi'_i}{\gamma_x(\cos\psi'_i+\beta_x)}, \quad (5)$$

where the incidence angle ψ'_i in Σ' is given by Eq. (2). Finally the field amplitude satisfies $E_r = E'_r\gamma_x(1+\beta_x\cos\psi'_i) = E''_r\gamma_x(\sec\psi'_i+\beta_x)$. Again $E''_r/\omega''_r = E'_r/\omega'_r = E_r/\omega_r$ is a Lorentz invariant.

As an important result, we find that, seen from the lab frame Σ, the light is reflected into an angle ψ_r much smaller than the angle of incidence ψ_i, depending on γ_x. This is shown in Fig. 2a, where ψ_r is plotted as a function of γ_x for $\psi_i = 30^o$ and 60^o. With the increase of γ_x, the reflected light turns strongly into the normal direction of the layer. For comparison, a layer at rest ($\gamma_x = 1$) would give simple specular reflection with $\psi_i = \psi_r$. Also the Doppler shift given by Eq. (4) depends on β_x and $\gamma_x = \sqrt{1-\beta_x^2}$ rather than the full β and γ of the individual electrons. Only for the special case $\gamma_x = \gamma$, the full Doppler shift $\omega_r/\omega_i = \gamma^2(1+\beta)^2$ can be reached for normal incidence. For oblique incidence, ω_r/ω_i is plotted as function of ψ_i in Fig. 2b for $\gamma_x = \gamma = 5$.

The present result holds for coherent scattering from a dense electron layer and is in distinct contrast to incoherent Thomson scattering which scatters the light into a direction close to that of the individual electron momenta. Even though all the relativistic electrons in the case studied here move into the same direction, their angle θ relative to the normal x-direction (see Fig. 1a) plays no apparent role in the coherent scattering process. The reason for this will become clearer in section 3, where we study the scattering itself in frame Σ''.

Lorentz transformations of p- and s-polarized light fields always lead to p- and s-polarized reflected fields, respectively, so the polarization states of incident and reflected wave remain the same. In the normal-incidence frame Σ'', there is no difference between p- and s-polarized fields, so that the field ratios E''_r/E''_i are same for both cases. Since field amplitude transformations are same for both polarization states, also the field ratio E_r/E_i in the lab frame is independent of the polarization states.

3 Coherent Thomson scattering

We are now in a position to calculate in frame Σ'' what fraction of incident light is reflected from the relativistic electron layer by coherent Thomson scattering. The layer has thickness d'' and electron density n''_e. The condition for coherent scattering is that many electrons reside in a volume λ''^3_i, i.e. $n''_e\lambda''^3_i \gg 1$. For the simple case of $\psi_i = 0$, this is equivalent to the condition

$$n_e \gg 10^{13}\gamma_x^4 cm^{-3} \quad (6)$$

in lab frame Σ. For $\gamma_x = 10$ and 100, coherent scattering requires $n_e \gg 10^{17}\mathrm{cm}^{-3}$ and $10^{21}\mathrm{cm}^{-3}$, respectively.

Let us now determine the reflectivity of such layers. For this we have to calculate the reflected amplitude E''_r from the incident amplitude E''_i for normal incidence in frame Σ''. The result has then to be transformed back to the lab frame Σ to obtain the reflection coefficient of photon energy and number. We start from the wave equation for the reflected light in plane 1D geometry

$$(\frac{\partial^2}{\partial x^2} - \frac{1}{c^2}\frac{\partial^2}{\partial t^2})A''_r(x,t) = S''(x,t) = -\mu_0 J''(x,t). \quad (7)$$

Here A''_r is the vector potential, and S'' is the source of the scattered radiation. It is given by the current $J''(x,t)$. We note that, in Eq. (7), the coordinates (x,t) refer also to frame Σ'', but for simpler notation we have dropped the double prime index. The incident laser field $E''_i(x,t) = E''_{i0}\sin(k''_i x + \omega''_i t)$ induces the linear current

$$J'' = -[e^2E''_{i0}n''_e(x)/\gamma'' m_e\omega''_i]\cos(k''_i x + \omega''_i t), \quad (8)$$

where $n''_e(x)$ is the electron density, γ'' the relativistic factor (see Sec. 2.2), m_e the rest mass, and $-e$ the charge of the electron. Notice that the uniform direct current related to the transverse velocities V''_y and V''_z is time-independent in the present model and does not contribute to the scattered radiation. The full electron velocity and its γ factor including the transverse component enters the source term of Eq. (7) only through the relativistic mass $\gamma'' m_e$. Also we consider here weak probe pulses only with amplitude $a_0 = eE''_{i0}/m_e c\omega''_i < 1$, which is the same in all frames. The small a_0 has negligible influence on γ''. Effects of non-linear Thomson scattering are not considered.

Another important assumption is made in deriving the current and should be emphasized. In taking a smooth electron density function $n''_e(x)$, rather than a random distribution of point electrons, we exclude incoherent scattering and suppose implicitly that the condition (6) for coherent scattering is fulfilled. In order to study the transition from incoherent to coherent scattering, the distribution of the individual scatterers has to be taken into account explicitly. This transition may become relevant in experiments, since the density profile of the layers decays in time. We expect that this will lead to significant changes in the scattered spectra with emission direction turning from normal x-direction to the direction of electron momenta and Doppler shifts changing from $4\gamma_x^2$ to $4\gamma^2$ scaling.

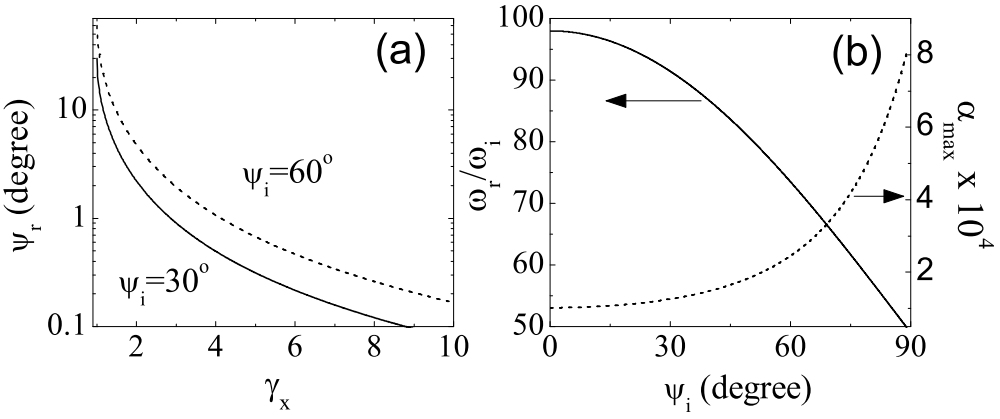

Fig. 2. (a) The reflection angle ψ_r as a function of γ_x for two angles of incidence, $\psi_i = 30^o$ and 60^o. (b) Frequency ω_r and maximum reflectivity $\alpha_{\max}$ as a function of the angle of incidence ψ_i. In both cases, it is set $\gamma_x = \gamma = 5$.

Equation (7) has the solution

$$A_r''(x,t) = \iint G(x-x', t-t')S(x',t')dx'dt', \qquad (9)$$

where $G(x-x', t-t') = -\frac{c}{2}H[(t-t') - |x-x'|/c]$ is the Green function of Eq. (7), and H is the Heaviside step function. Equation (9) leads to

$$A_r''(x,t) = -\frac{c}{2}\int_{-\infty}^{\infty} dx' \int_{-\infty}^{t-|x-x'|/c} S(x',t')dt'. \qquad (10)$$

¿From Eq. (10), one obtains the electric field

$$E_r'' = -\frac{\partial A_r''}{\partial t} = \frac{c\mu_0 e^2 E_{i0}''}{2\gamma'' m_e \omega_i''} \times \int_{-\infty}^{\infty} n_e'' \cos[k_i''x' + \omega_i''(t-|x-x'|/c)]dx'. \qquad (11)$$

For simplicity, we consider an electron slab with uniform density $n_e''(x) = n_{e0}''H(-x)H(x+d'')$. For the reflected wave propagating in $+x$ direction, Eq. (8) leads to

$$E_r''(x,t) = \frac{e^2 n_{e0}'' E_{i0}''}{2m_e\varepsilon_0\gamma''\omega_i''^2}\sin\xi\cos(\omega_i''t - k_i''x - \xi), \qquad (12)$$

where $\xi \equiv k_i''d''$. Making use of the relations derived in Section 2, the field $E_r''(x,t)$ is now transformed back into the lab frame, where $E_r(x,t) = E_{r0}\cos(\omega_i t - k_i x - k_i''d'')$ is obtained with the amplitude

$$E_{r0} = E_{i0}\frac{\omega_{p0}^2}{2\omega_i^2}\frac{(\sec\psi_i' + \beta_x)\sin\xi}{\gamma(1+\beta_x\cos\psi_i)\cos\psi_i'}. \qquad (13)$$

Here $\omega_{p0} = \sqrt{e^2 n_{e0}/m_e\epsilon_0}$ is the plasma frequency, and $\xi = k_i d\gamma_x^2(1+\beta_x\cos\psi_i)\cos\psi_i'$.

Taking into account the ratio of pulse durations of incident and reflected wave which is given by $\tau_r/\tau_i = \omega_i/\omega_r$, Eq. (13) allows to calculate the fraction of pulse energy reflected by the relativistic electron layer:

$$\alpha = \frac{E_{r0}^2\tau_r}{E_{i0}^2\tau_i} = \frac{\omega_{p0}^4}{4\omega_i^4}\frac{(1+\beta_x\cos\psi_i')\sin^2\xi}{\gamma^2\gamma_x^2(1+\beta_x\cos\psi_i)^3\cos^4\psi_i'}. \qquad (14)$$

This is the central result of the present paper. We call α the reflectivity for coherent Thomson scattering. Notice that $\alpha \propto \omega_{p0}^4/\gamma^2 \propto n_{e0}^2/(\gamma m_e)^2$. Apparently, it depends quadratically on the layer density, as it should be for coherent scattering, and on the full γ factor exclusively through the relativistic mass γm_e. Another remarkable feature is that the direction of electron motion defined by the angle θ plays no special role. In contrast to incoherent scattering, the coherently scattered radiation exhibits no conspicuous maxima when choosing $\psi_i = \theta$ and $\phi = \pi$ (see discussion about φ below), in which case the probe radiation is incident just head-on to the electron momenta.

Instead α depends explicitly on the normal velocity component β_x, $\gamma_x = (1-\beta_x^2)^{-1/2}$, and kinematic factors related to oblique incidence. This is also true for the factor $\sin^2\xi = \sin^2(k_i''d'') = \sin^2(\pi d/L)$, describing oscillations of the reflectivity as a function layer thickness d. The period of these oscillations is given by $L = \lambda_i/[2\gamma_x^2(1+\beta_x\cos\psi_i)\cos\psi_i'] \approx \lambda_r$, i.e. the wavelength of the reflected radiation in the lab frame. The periodic modulation of α with d is due to coherent superposition of radiation scattered from different depths of the electron layer. It is shown for normal incidence and $\gamma_x = \gamma = 5$ in Fig. 3a. The first maximum shows up for $d = \lambda_r/2$ and minima at $d = \lambda_r, 2\lambda_r, \ldots$. In Fig. 2b, the maximum reflectivity $\alpha_{\max}$ is plotted versus angle of incidence ψ_i; for the oblique incidence, the reflectivity increases, while the frequency of the reflected radiation decreases.

We also point out that the reflection frequency ω_r, angle ψ_r and reflectivity α are all independent of the azimuthal angle φ, i.e. the direction of the transverse velocity of the mirror. In Fig. 1a, one can simply set φ to zero or π. However, the azimuthal angle φ is contained in n_e'', which has an influence on the criterion in Eq. (6), provided that $\psi_i \neq 0$.

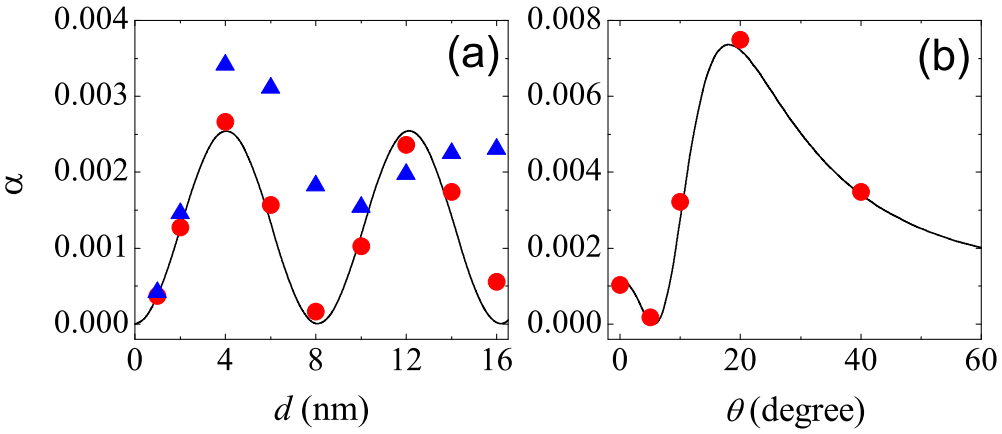

Fig. 3. (Color online) Reflectivity α for $\gamma = 5$, $\psi_i = 0$, and $n_{e0} = 5n_c$. The analytical result (solid line, Eq. (15)) is compared with PIC simulations: (a) dependence on layer thickness d for $\gamma_x = \gamma = 5$ ($\theta = 0$), (b) dependence on electron direction θ for fixed $d = 10$ nm. Few-cycle cosine-type pulses were used in the simulation with duration $T = 8\tau_i$ (circles) and $T = 3\tau_i$ (triangles).

For normal incidence with $\psi_i = 0$, expression (14) for α reduces to

$$\alpha(\psi_i = 0) = \frac{\omega_{p0}^4}{4\omega_i^4} \frac{\sin^2[\gamma_x^2(1+\beta_x)k_i d]}{\gamma^2\gamma_x^2(1+\beta_x)^2}. \qquad (15)$$

The reflection coefficient of photon number is a Lorentz invariant and is easily obtained in the form

$$\alpha_{ph} = \alpha\frac{\omega_i}{\omega_r} = \frac{\omega_{p0}^4}{4\omega_i^4} \frac{\sin^2\xi}{\gamma^2\gamma_x^4(1+\beta_x\cos\psi_i)^4\cos^4\psi_i'}. \qquad (16)$$

In the limit $\psi_i = 0$ and $\xi \ll 1$, we find

$$\alpha_{ph} \approx (n_{e0}k_i d/4n_c\gamma)^2, \qquad (17)$$

where n_c is the critical density corresponding to frequency ω_i. This result is also contained in Ref. [2]. One should realize, however, that the condition $\xi \ll 1$, i.e. $d \ll \lambda_r/\pi$, is difficult to fulfil experimentally, in particular for higher values of γ_x.

4 PIC simulation

We have performed 1D PIC simulation to check the mirror reflectivity α derived above. For a direct comparison, we have introduced an ion background in the simulation, moving synchronously with the electron layer to suppress Coulomb expansion. This charge-compensating background has almost no effect on the Thomson scattering because of the high ion mass. In the simulation, the probe laser pulse is perpendicularly incident ($\psi = 0$) and has amplitude $a_0 = eE_{i0}/m_e c\omega_i = 0.01$, wavelength $\lambda_i = 800$ nm, and a $\sin^2(t/T)$ envelope. Two different pulse durations, $T = 8\tau_i$ and $T = 3\tau_i$, were used.

Comparisons with the analytical results are shown in Fig. 3. In Fig. 3a, α is plotted versus layer thickness d for fixed $\gamma_x = \gamma = 5$ ($\theta = 0$). The modulation due to constructive and destructive interference is well reproduced by the simulated results for the longer pulse duration (circles), but for the short ($T = 3\tau_i$, triangles) pulse agreement is found for $d \ll 4$ nm below the first maximum of α. The reason is incomplete destructive interference for very short pulses due to time delay of reflected signals from deeper layers. It is found that the reflectivity saturates for thicker layers at almost the level of the first maximum. In Fig. 3b, we kept $d = 10$ nm and $\gamma = 5$ fixed and varied the inclination angle θ of electron momenta relative to x direction. Again, we find perfect agreement between simulated long pulse results and Eq. (15).

Finally, we compare with a more realistic PIC simulation (no artificial ion background). In this case, we have to extract space- and time-averaged density values from the simulation approximately and cannot expect quantitative agreement with the analytical results. Nevertheless, the analytical results prove useful for understanding qualitative behavior. Results are shown in Fig. 4 and Table 1.

Similar to cases discussed in paper I, we consider a foil, initially 5 nm thick and having a density of $n_{e0}/n_c = 1$, and irradiate it by a drive laser pulse of form $a_d \sin(\omega_i t)$ with sharp front and $a_d = 2$. This is sufficient to drive out all electrons from the foil and to generate a thin electron layer. It reaches $\gamma \approx 8$ and $\gamma_x \approx 2$ after two laser cycles of laser interaction, as it is seen in Fig. 4a. At this point of time, we let the electron layer interact with a counter-propagating half-cycle switch pulse (see detailed discussion in paper I) of the form $-a_s \sin(\omega_i t)$ with $a_s = 1.9$. This switch pulse turns electron momenta into x direction such that $\gamma_x = \gamma \leq 7.9$ for a longer period of time. In this way we have prepared a relativistic mirror to test the reflectivity α.

A 15-cycle flat-top probe pulse is chosen with normal incidence, $a_0 = 0.01$, and polarized orthogonal to the drive pulse. Both drive and probe pulse touch the foil at same time $t = 0$. The reflected probe signal is shown in Fig. 4b and its power spectrum in Fig. 4c. It is detected at

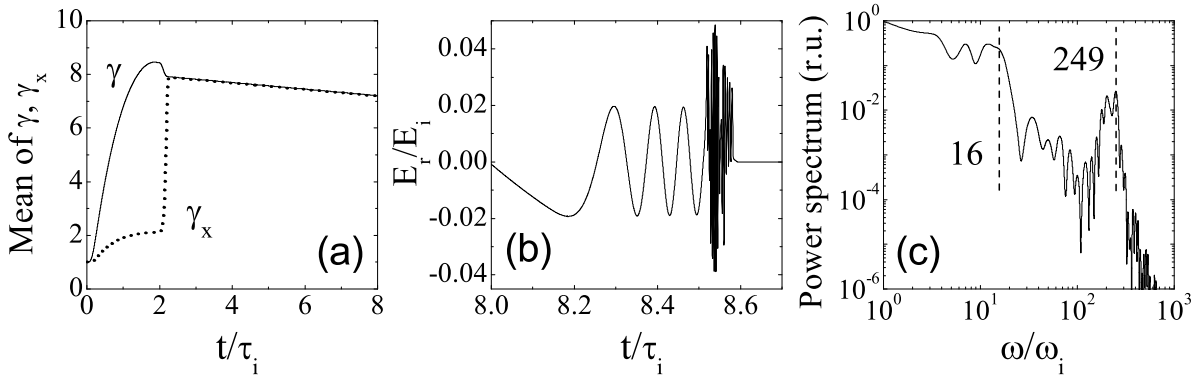

Fig. 4. Results of PIC simulation of probe laser ($a_p = 0.01$) reflection from ultrathin foil ($d = 5$ nm, $n_e/n_c = 1$), irradiated by drive laser pulse with $a_d = 2$ and half-cycle switch pulse. (a) Time evolution of γ and γ_x averaged over electron layer. (b) Reflected signal. (c) Corresponding power spectrum. For details see text.

Table 1. Fractions of probe light energy reflected before and after switch pulse. Comparison of simulated results with Eq. (15).

	before switch	after switch
simulation	5.23×10^{-5}	5.55×10^{-6}
analytic (Eq. (15))	3.96×10^{-5}	3.59×10^{-6}

a position of $8\lambda_L$ behind the foil. In Fig. 4b we see that about 3.5 cycles of probe light are reflected before the switch pulse hits. In this early phase, γ_x is increasing up to a value of 2.1 . It produces the chirped part of the reflected pulse, seen for $t/\tau_i \leq 8.52$, and the low-frequency plateau in the spectrum extending up to $\gamma_x^2(1+\beta_x)^2 \approx 16$. Then the switch pulse abruptly changes the reflected signal. Fast oscillations show up and generate the high-frequency peak in the spectrum at $\omega/\omega_i \approx 4\gamma^2 \approx 249$, corresponding to $\gamma \approx 7.9$.

We have extracted the reflectivities from the simulation for the time intervals before and after switch pulse impact. At this point of time, the layer density $n_e/n_{e0} = d_0/d$ is estimated from its thickness $d = 6.4$ nm; time-averaged values for γ_x and γ are chosen. Results are compared with analytic values in table 1. One recognizes that Eq. (15) describes the simulated reflectivities fairly well for two significantly different sets of mirror parameters. The deviations are within a factor of two and can be attributed to the averaging over temporal changes in layer evolution.

5 Conclusions

In conclusion, we have investigated linear coherent Thomson backscattering of probe radiation obliquely incident on ultra-thin dense electron layers. They act as relativistic mirrors. In particular, the present investigation is related to laser irradiation of ultra-thin foils in a regime in which all electrons are separated from ions and driven to form the relativistic mirror. Here an analytical expression for the mirror reflectivity has been derived and verified by comparison with 1D PIC simulations.

The direction of the coherently reflected light is oriented along the normal direction of the plane layer, which is also the direction of the driving laser pulse. Different from incoherent scattering, it is not oriented along the electron momenta. In the case of direct laser electron acceleration considered here, electron momentum has necessarily a transverse component p_y and is inclined relative to the normal direction. Even tough all these angles become small for $\gamma \gg 1$, a significant difference remains with respect to Doppler shifts, which scale $\propto \gamma_x^2 = \gamma^2/(1+(p_y/m_e c)^2)$ rather than $\propto \gamma^2$. This typically leads to spectra lower in frequency for coherent scattering, though much higher in intensity. In thin foil experiments, the transition from coherent to incoherent scattering may be detected when the layer density decays in time.

The mirror reflectivity derived in this paper is also governed by γ_x. For oblique incidence, it is found to be almost independent of p- or s-polarization; reflectivity rises with angle of incidence, while frequency falls. The coherent reflectivity oscillates as a function of layer thickness due to constructive and destructive interference of light reflected at different layer depth. This modulation is damped for ultra-short few-cycle pulses due to time delay of reflections from different depth.

In summary, light reflected coherently from relativistic electron layers is expected to become an important new source of VUV- and X-radiation. It will also serve as an excellent tool to diagnose layer electron evolution.

Acknowledgments

H.-C. Wu acknowledges support from the Alexander von Humboldt Foundation. This work was also supported by the DFG project Transregio TR18, by the Munich Centre for Advanced Photonics (MAP), and by the Association EURATOM - Max-Planck-Institute for Plasma Physics.

References

1. A. Einstein, Ann. Phys. (Leipzig) **17**, 891 (1905).
2. S.V. Bulanov, T. Esirkepov, T. Tajima, Phys. Rev. Lett. **91**, 085001 (2003)
3. A.S. Pirozhkov et al., Phys. Plasmas **14**, 123106 (2007).
4. R. Lichters, J. Meyer-ter-Vehn, A. Pukhov, Phys. Plasmas **3**, 3425 (1996).
5. S. Gordienko et al., Phys. Rev. Lett. **93**, 115002 (2004).
6. T. Baeva, S. Gordienko, A. Pukhov, Phys. Rev. E **74**, 046404 (2006).
7. B. Dromey, et al., Phys. Rev. Lett. **99**, 085001 (2007).
8. V.A. Vshivnov, N.M. Naumova, F. Pegoraro, S.V. Bulanov, Phys. Plasmas **5**, 2727 (1998).
9. A.S. Pirozhkov, S.V. Bulanovet, T.Zh. Esirkepov et al., Phys. Plasmas **13**, 013107 (2006).
10. J. Meyer-ter-Vehn and H.-C. Wu, Eur. Phys. J. D (2008), contribution to this volume.
11. V.V. Kulagin, V.A. Cherepenin, M.S. Hur, H. Suk, Phys. Rev. Lett. **99**, 124801 (2007).
12. E. Esarey, S.K. Ride, P. Sprangle, Phys. Rev. E **48**, 3003 (1993).
13. H. Schwoerer, B. Liesfeld, et al., Phys. Rev. Lett. **96**, 014802 (2006).
14. A. Bourdier, Phys. Fluids **26**, 1804 (1983).